ACS APPLIED MATERIALS & INTERFACES

Research Article

www.acsami.org

Solid-State Photogalvanic Dye-Sensitized Solar Cells

Seare A. Berhe, Habtom B. Gobeze, Sundari D. Pokharel, Eunsol Park, and W. Justin Youngblood*

Department of Chemistry, University of North Texas, Denton, Texas 76203, United States

Supporting Information

ABSTRACT: Photogalvanic cells are photoelectrochemical systems wherein the semiconductor electrode is not a participant in primary photoinduced charge formation. The discovery of photoelectrochemical systems that successfully exploit secondary (thermal) electron injection at dye−semiconductor interfaces may enable studies of electron transfer at minimal driving force for electron injection into the semiconductor. In this study, we have examined thermal electron transfer from molecular sensitizers to nanostructured semiconductor electrodes composed of titanium dioxide nanorods by means of transient spectroscopy and the assembly and testing of photoelectrochemical cells. Electron-accepting molecular dyes have been studied alongside an arylamine electron donor. Thermal injection is estimated for a naphthacenequinone radical anion as a multiexponential decay process with initial decay lifetimes of 6 and 27 ps. The ambient electric field present during charge separation at a surface-adsorbed dye monolayer causes Stark shifts of the radical ion pair absorbance peaks that confounded kinetic estimation of thermal injection for a fullerene sensitizer. Electron-accepting dyes that operate by thermal injection into titanium dioxide function better in solid-state photoelectrochemical cells than in liquid-junction cells due to the kinetic advantage of solid-state cells with respect to photoinduced acceptor-quenching to form the necessary radical anion sensitizers.

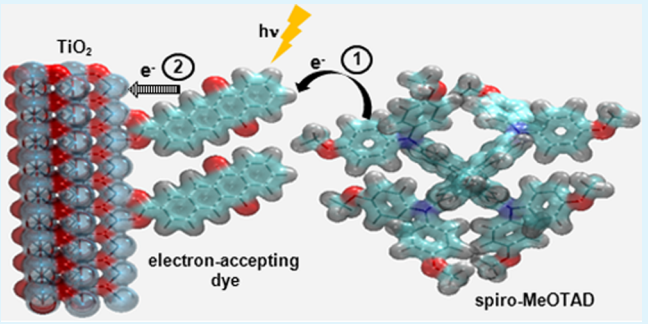

KEYWORDS: *photogalvanic, dye-sensitized, solar cells, thermal, electron, transfer*

INTRODUCTION

Photogalvanic cells (PSCs) produce electrochemical potential by the photoinitiated perturbation of a redox equilibrium between donor and acceptor compounds in an electrolyte (Figure 1).[1,2] The most well-studied redox pair in such cells has been the iron-thionine system. Photogalvanic potential within the electrolyte is communicated to the collecting electrodes. Recombination is reduced by use of an n-type semiconductor as the electron-collecting electrode. Nevertheless, significant kinetic competition remains between charge transfer to the electrodes versus charge recombination among dissolved redox carriers. Suppressing the solution-phase recombination requires minimal cell thickness (<10 μm) such that optical absorption is too limited to efficiently harvest ambient solar irradiation.[3]

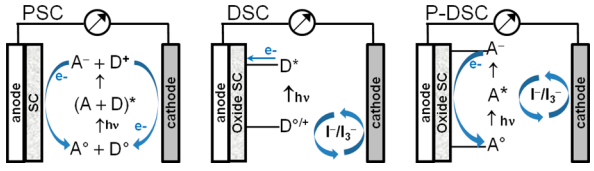

Figure 1. Schematic diagrams of solar cell types: photogalvanic ("PSC", left), dye-sensitized ("DSC", center), and photogalvanic dye-sensitized ("P-DSC", right). Within diagrams: SC = semiconductor; D = donor; A = acceptor; $h\nu$ = photoexcitation; e^- = electron; I^-/I_3^- = iodide/triiodide.

Modern organic photovoltaic solar cells, wherein charge separation occurs in a photoactive layer of organic semiconductor material and must migrate to collecting electrodes,[4] can be regarded as solid-state photogalvanic cells.

Dye-sensitized solar cells (DSCs) rely on charge injection from photoexcited surface-adsorbed dyes into wide band gap oxide semiconductors; and similar to photogalvanic cells, DSCs also suffered from poor light absorption until the shift was made from planar to mesoporous semiconductor electrodes as first reported by Gratzel and now widely followed.[5,6] Photogalvanic dye-sensitized solar cells (P-DSCs), as studied by the Ortmans and Meyer groups,[7−11] are a hybrid of the dye-sensitized and photogalvanic paradigms: primary charge separation occurs between molecular donor−acceptor pairs, with thermal electron donation by photoreduced surface-adsorbed sensitizers into a wide band gap oxide semiconductor (Figure 1). The surface adsorption of electron-accepting dyes onto nanostructured oxide semiconductors allows for enhanced light absorption while reducing recombination between the primary donor/acceptor pair by removing one of these components (the acceptor) from the electrolyte.

Whereas photoinduced electron injection within DSCs may occur from thermally relaxed or upper excited states,[12,13]

Received: April 24, 2014
Accepted: May 29, 2014
Published: May 29, 2014

Chart 1. Fullerene and Naphthacenequinone Acceptor-Sensitizers

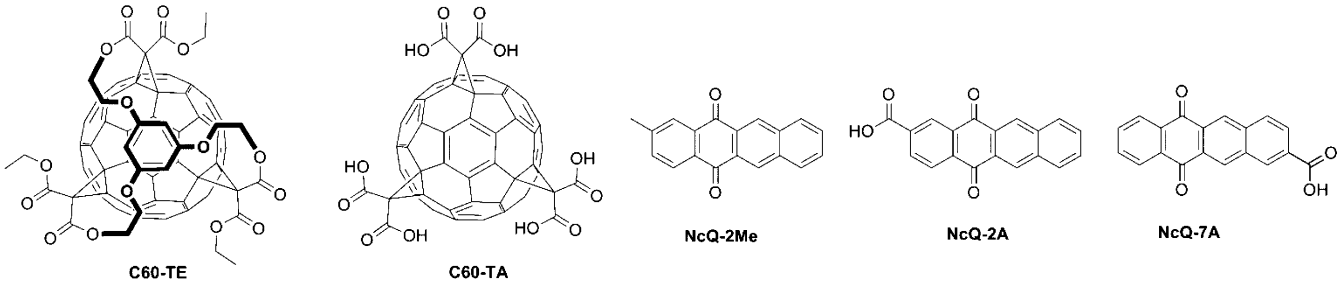

thermal electron injection mode within P-DSCs occurs from only a single state, the radical anion state of the bound sensitizer. The relatively simpler injection kinetics of P-DSCs compared to DSCs should make P-DSCs an attractive model system for studying electron transfer rates at precise energetic relationships between the adsorbed dyes and the acceptor states of n-type semiconductors. Such studies may be useful in reducing the energy lost as overpotential in the electron injection event. Because thermal electron injection rates at dye/oxide interfaces should be somewhat insensitive to the nature of the primary donor species, the P-DSC paradigm may also provide a reliable injection pathway for some photoactive donor-dyes that exhibit slow electron injection when used as directly adsorbed sensitizers in DSCs.[14−17] Despite these advantages, the field of study into the operation of P-DSC devices remains small, certainly in comparison to that of DSC research.

Reported studies of photogalvanic dye-sensitized solar cells up to the present time include both intentionally designed and accidentally discovered systems. Meyer and co-workers reported a ruthenium polypyridyl sensitizer that exhibited acceptor quenching and rapid ($k > 10^9$ s^{-1}) thermal electron injection into titanium dioxide (TiO_2), although the precise rate constant for the thermal process was not determined.[8] Nanosecond-time scale transient spectroscopy studies have been unable to directly measure the kinetics of thermal electron transfer, even for some donor−acceptor dyads designed to probe the process.[10,11] A number of optoelectronically tuned ruthenium dyes that can exhibit acceptor quenching without thermal electron injection have proven useful in the determination of fundamental metrics of electron transfer such as the kinetics of acceptor-quenching of dyes by dissolved redox shuttles.[18−20] Such studies have brought considerable insight into the mechanism for the regeneration of photo-oxidized dyes by the iodide/triiodide electrolyte in DSCs. Boschloo and co-workers reported a perylenediimide sensitizer that worked better in solid-state DSCs than in liquid junction photocells, suggesting different pathways for electron transfer across different environmental conditions.[21,22] Significant overlap of absorption patterns among the ground, excited, oxidized, and reduced forms of the dye, along with Stark shifts in the spectra caused by the electric field present upon electron injection into the semiconductor (TiO_2) complicated the understanding of the dye's electron transfer behavior. More recently, D'Souza and co-workers reported a supramolecular porphyrin−phthalocyanine dyad at TiO_2 surface with photophysical behavior suggesting that primary electron transfer from phthalocyanine to porphyrin preceded electron injection into TiO_2, although overlaps in the spectral traces of the two tetrapyrroles hindered precise determination of rates for the observed processes.[23]

We have previously examined thermal electron injection by acceptor-sensitizers such as fullerene and acenequinone dyes into TiO_2 and ZnO at the polymer/oxide interface of hybrid inverted organic solar cells.[24] Despite the lower surface area of our oxide nanorod films compared to mesoporous oxide electrodes, we observed photosensitization by adsorbed acceptor-dye. The polymer/dye/oxide solar cells can be viewed as a solid-state version of a P-DSC, with poly(3-hexylthiophene) acting both as a photoactive primary donor and a hole-conducting substitute for electrolyte. To better understand the photosensitization behavior of fullerene and acenequinone dyes, we have herein conducted a study of electron transfer between the transparent arylamine donor spiro-MeOTAD and TiO_2, mediated by fullerene and acenequinone sensitizers at the donor/oxide interface. We have separately examined the electron transfer in binary donor−acceptor and ternary donor−acceptor−TiO_2 systems using transient absorbance spectroscopy. We have also assessed the photoelectrochemical behavior of these sensitizers across solid-state and liquid junction solar cells. We present some of the strongest evidence to date for successful thermal electron transfer into an oxide semiconductor, and we propose that solid-state P-DSCs are a more facile system for exploring this phenomenon compared to liquid junction photocells.

EXPERIMENTAL SECTION

Chemicals were purchased as reagent grade and used as received. *N*-methylpyrrolidinone (NMP) was dried over molecular sieves. Compounds NcQ-2Me, C60-TE, and C60-TA (Chart 1) were available from our previous preparation.[24] 3,4-Bis(dibromomethyl)-benzoic acid was prepared as previously described.[24,25] Analytical data were consistent with the previous results. UV−vis absorption data were collected with a Varian Cary spectrophotometer.

5,12-Naphthacenequinone-7-carboxylic Acid (NcQ-7A). A 10 mL round-bottom flask was charged with 3,4-bis(dibromomethyl)-benzoic acid (784 mg, 1.68 mmol), naphthoquinone (266 mg, 1.68 mmol), and NaI (504 mg, 3.36 mmol). The flask was sealed with a septum and purged with argon, and then NMP (2.0 mL) was added. The mixture was heated to 80 °C for 3 h, and a color change to red was observed. The reaction mixture was allowed to cool to room temperature, and a 5% aq soln of $NaHSO_3$ (10 mL) was added, whereupon the red color dissipated and a yellow precipitate appeared. The solid was filtered and washed with water, then dissolved in 1 M aq NaOH and the resulting yellow solution was filtered. The filtrate was acidified with 4 M HCl, regenerating a yellow precipitate that was filtered and dried under vacuum to give the product as a yellow solid (325 mg, 64%). δH (400 MHz, $(CD_3)_2SO$): 7.96−8.01 (m, 2H), 8.20 (dd, J_1 = 8.6 Hz, J_2 = 1.6 Hz, 1H), 8.28−8.33 (m, 2H), 8.42−8.46 (m, 1H), 8.94 (s, 1H), 8.97−8.99 (m, 1H), 9.06−9.07 (m, 1H), 13.46 (br s, 1H); δC (125 MHz, $(CD_3)_2SO$): 127.10, 128.60, 128.63, 130.21, 130.49, 130.59, 131.13, 131.36, 131.40, 132.40, 133.99, 134.01, 134.06, 134.73, 134.79, 136.52, 141.89, 166.88, 182.13, 182.29. UV−vis ($CHCl_3$) λ_{max}(nm): 295, 396.

Preparation of TiO_2 Nanorod Films. Conductive glass substrates (F-SnO_2 on soda lime glass, Pilkington Glass Tec-7) were patterned by chemical etching using Zn dust and 4 M HCl. Substrates were then sonicated in acetone, ethanol, and deionized water for 5 min respectively, air-dried in a laminar flow hood and treated in an ozone cleaner for 15 min. Following a reported procedure,[26] substrates were passivated by thermal evaporation of Ti^0 metal to 100 Å thickness, annealed at 450 °C for 30 min under ambient atmosphere, and then TiO_2 nanorod films were grown hydrothermally by placing the substrates in a solution of $Ti(iOPr)_4$ (28 mM) in aq HCl (5 M) inside a Teflon chamber within a stainless steel Parr vessel placed in an oven at 150 °C. Growth was conducted for 6 h, after which the Parr vessel was removed and cooled for several minutes under a stream of tap water. TiO_2 nanorod films were removed from the growth bath and gently rinsed with deionized water and air-dried. A scanning electron micrograph of a representative film is shown in the Supporting Information.

Preparation of Films for Transient Spectroscopy Studies. For binary donor–acceptor studies, toluene solutions of spiro-MeOTAD blended with either C60-TE or NcQ-2-Me were spin-coated onto glass sides. For ternary donor–acceptor-TiO_2 studies, TiO_2 nanorod films were soaked in organic solvent containing either C60-TA (DMF) or NcQ-7A (EtOH) overnight and then rinsed with solvent and air-dried. Each dye-coated TiO_2 film was covered by a toluene solution containing spiro-MeOTAD for 30 s and then spun on a spin-coater at 1200 rpm for 45 s.

Femtosecond Transient Absorption Spectral Measurements. Transient absorption spectroscopy was performed using an ultrafast femtosecond laser source (Libra by Coherent) incorporating a diode-pumped, mode locked Ti:sapphire laser (Vitesse) and diode-pumped intra-cavity doubled Nd:YLF laser (Evolution) to generate a compressed laser output of 1.45 W. For optical detection a Helios transient absorption spectrometer coupled with a femtosecond harmonics generator (Ultrafast Systems) was used. The source for the pump and probe pulses were derived from the fundamental output of the laser (pulse width 91 fs) at a repetition rate of 1 kHz. 95% of the fundamental output of the laser was introduced into the harmonic generator, which produces second and third harmonics of 400 and 267 nm besides the fundamental 800 nm for excitation, while the rest of the output was used for generation of white light continuum. In the present study, the second harmonic 400 nm excitation pump was used in all the experiments. Kinetic traces at appropriate wavelengths were assembled from the time-resolved spectral data. All measurements were conducted at 298 K.

Device Assembly and Testing. Sensitization of oxide substrates was performed by soaking the TiO_2 nanorod films overnight. For liquid cells, a solution of spiro-MeOTAD (170 mM), 4-*tert*-butylpyridine (130 mM), $LiN(CF_3SO_2)_2$ (13 mM), and tris(4-bromophenyl)-aminium hexachloroantimonate (0.3 mM) in chlorobenzene was applied to the sensitized TiO_2 nanorod films by leaving the solution to penetrate into the film for 45 s and then spin-coating for 40 s with 1200 rpm. PEDOT:PSS was spin-coated from aqueous dispersion. Films were transferred into a metal evaporator and silver electrodes of ~70 nm thickness were deposited in island-type geometry with a central dot of 1.1 cm^2 area. Ag paste was applied to improve electrical contact at electrode edges, and allowed to dry overnight in an oven at 50 °C. Devices were tested on the day after they were assembled. Current–voltage measurements were taken with a sourcemeter (Keithley 2400) and a Class A solar simulator (Solarlight, Inc.). IPCE spectra (incident photons converted to electrons) were measured against a calibrated silicon photodiode using monochromatic light from a xenon lamp (PV measurements QEX7). For liquid-junction cells, counterelectrodes were prepared by applying a drop of H_2PtCl_6 solution (5 mM in iPrOH) on FTO glass, air drying, and annealing at 380 °C for 30 min. Two pieces of Surlin film were sandwiched between the sensitized electrode and the counterelectrode, and the two electrodes were sealed with the film using a heated press. A drop of an electrolyte (0.1 M LiI, 0.05 M I_2, 0.6 M 1,2-dimethyl-3-propylimidazolium iodide, 0.5 M *tert*-butylpyridine in CH_3CN) was applied at a gap between the Surlin films and was allowed to enter and fill the inside volume through capillary action. The entry/exit ports were then sealed with epoxy (Hysol 1C). Devices were tested on the same day that they were assembled, using the same instrumentation as for solid-state photoelectrochemical cells.

RESULTS AND DISCUSSION

Synthesis and Optoelectronic Properties of Acceptor-Sensitizers. Based on our previous results with fullerene and acenequinone acceptor-sensitizers, we decided to examine trisadduct fullerene and naphthacenequinone dyes for this study (Chart 1). We prepared the naphthacenequinone-carboxylic acid NcQ-7A as a replacement for the similar compound NcQ-2A used in our previous study of polymer/oxide semiconductor interfaces. NcQ-2A requires a four-step synthesis from commercially available starting materials, with some batch variability in the final chromic acid-mediated benzylic oxidation of 2-methylnaphthacenequinone (NcQ-2Me). NcQ-7A is available in two steps from commercially available reagents with excellent reproducibility (Scheme 1).

Scheme 1. Synthesis of NcQ-7A

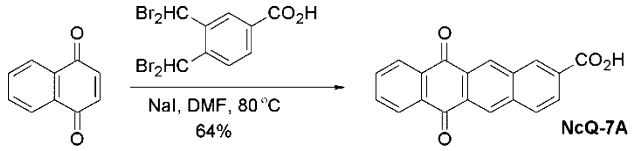

Redox potentials for the neutral photoexcited and radical anion states of the acceptor-sensitizers NcQ-7 and C60-T are shown in Table 1, along with the effective flat band potential of

Table 1. Redox Potentials of Organic Semiconductors and Conduction Band Edge of TiO_2[a]

substance	ESOP$^{(*/+)}$	$E^{\circ}_{A/A-}$/CB	ref.
NcQ-7[b]	$^{S}-1.08/^{T}-0.57$	−1.13[c]	29
C60-T	$^{S}-0.44/^{T}-0.17$	−0.86[c]	30
TiO_2 (dry)		−0.5/−0.25[d]	31, 32

[a]All potentials determined for solvated species vs SCE or converted to SCE from other electrodes[33] or vacuum level,[34] where indicated. ESOP = Excited State Oxidation Potential. $E^{\circ}_{A/A-}$ = reduction potential. CB = conduction band edge. ^{S} Singlet excited state. ^{T} Triplet excited state. [b]Reported for 5,12-naphthacenequinone. [c]Originally reported for ester derivative. [d]Originally reported vs vacuum (Kelvin probe).

TiO_2 in the dry state as reported in two different studies. Given that the molecular species were characterized in solution, we expect that their redox potentials may be different in the dry, surface-adsorbed environment of a solid state P-DSC. Optimistically taking the measured redox potentials of the dyes as indicative of their expected behavior in solid-state P-DSCs, we note that NcQ-7A would be capable of electron injection from either its singlet or triplet neutral photoexcited state, whereas C60-TA would only be capable of electron injection from its singlet excited state, which has a reported lifetime of 3.1 ns.[27] Singlet excited naphthacenequinone is known to undergo intersystem crossing at the femtosecond time scale;[28] however, ultrafast electron injection into TiO_2 has been reported for some dyes.[5]

Transient Absorbance Spectroscopy of Binary and Ternary Systems. Photoinitiated charge separation and thermal recombination were characterized for thin film blends

of the NcQ-2Me and C60-TE acceptors with spiro-MeOTAD. Schematics of the electron transfer processes in binary and ternary systems are shown in Figure 2. Photoinduced acceptor-

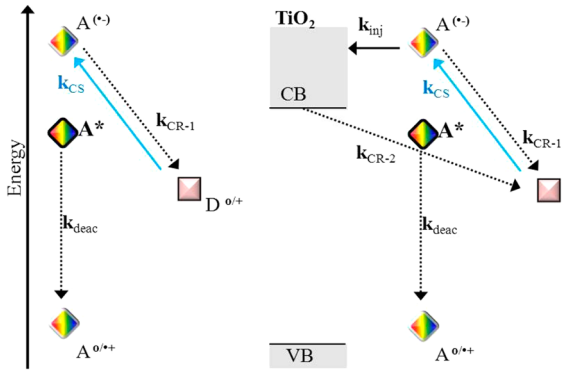

Figure 2. Schematics of the electron transfer processes in binary donor–acceptor (left) and ternary donor–acceptor–TiO_2 (right) systems. $A^{o/\bullet+}$ = ground state acceptor; A* = photoexcited acceptor; $A^{(\bullet-)}$ = acceptor radical anion; $D^{o/\bullet+}$ = ground/oxidized donor; VB = valence band; CB = conduction band; k_{CS} = charge separation; k_{CR-1} = bimolecular recombination; k_{inj} = thermal electron injection; k_{CR-2} = oxide-to-donor recombination.

quenching to form a radical anion with electrochemical potential that is negative of the neutral photoexcited state can be formed under exothermic conditions, so long as the energy of the excited state ($E_{0,0}$) is sufficient to compensate for the resulting electrochemical potential of the radical ion pair ($E^{\circ}_{D/D^+} - E^{\circ}_{A/A^-}$) and any solvent/environment reorganization (ΔG_S), as shown in eq 1.[35]

$$\Delta G^{\circ} = (E^{\circ}_{D/D^+} - E^{\circ}_{A/A^-}) - E_{0,0} + \Delta G_S \quad (1)$$

Time-resolved spectra of the charge separated pair NcQ-2Me/spiro-MeOTAD are shown in Figure 3A. The peak centered near 600 nm represents the naphthacenequinone radical anion,[36] whereas the peaks centered near 500 and 750 nm correspond to the spiro-MeOTAD radical cation.[37,38] Charge separation appears complete within 1 ps of the laser pulse, and the multiexponential decay rates of these peaks track closely (Figure 3B and Table 2). There is an initial offset of the radical anion decay caused by a rapid decay component ($\tau \sim 1$ ps) which we attribute to electron transfer to ambient gas-phase oxygen. The matching decay traces otherwise suggest a simple binary charge separation/recombination system.

Flash photolysis of a C60-TE/spiro-MeOTAD blend film (Figure 4) also shows charge separation complete within 1 ps, as well as the very fast initial decay (~1 ps) for just the radical anion that we assign as electron transfer to ambient oxygen. Although the calculated decay rates for the charge separated pair (Table 3) seem quite distinct, we note that the τ_2 and τ_3 time constants for $C60\text{-}TE^{(\bullet-)}$ have large uncertainties and the decay traces for the radical pair match perfectly if normalized at 5 ps (Supporting Information Figure S1). We had expected that recombination in the C60-TE/spiro-MeOTAD system would be much slower than for the NcQ-2Me/spiro-MeOTAD pair because the Marcus kinetics (eq 2) impart significant impact for the reorganization energy (λ), which is known to be much lower for fullerenes (~0.4 eV) than for quinones (~0.9 eV).[39,40] Equation 2 provides a parabolic relationship between enthalpic driving force and electron transfer rates, with fastest electron transfer occurring where $\lambda = \Delta G^{\circ}$. As enthalpic driving force exceeds the reorganization energy, electron transfer slows, so a smaller λ is expected to lead to easier attainment of such "Marcus inverted" conditions for delayed recombination.[41] Comparing the decay rates for spiro-MeOTAD across the two binary systems, it appears that the decay is slightly slower for the NcQ-2Me system. A possible explanation for this surprising result may be that the C60-TE is likely to accomplish efficient acceptor-quenching from its singlet excited state, whereas the NcQ-2Me may undergo intersystem crossing prior to acceptor-quenching, thereby accessing a triplet charge separated state for which the recombination is a spin-forbidden process.[42]

$$k_{ET} = \frac{2\pi}{\hbar}|V|^2 \frac{1}{4\lambda k_B T} e^{\left[\frac{-(\lambda+\Delta G^{\circ})^2}{4\lambda k_B T}\right]} \quad (2)$$

Equation 2 shows the Marcus electron transport kinetics where V = coupling constant, k_B = Boltzmann constant, λ = reorganization energy, ΔG° = enthalpic driving energy.

Laser flash photolysis of the ternary system TiO_2/NcQ-7A-spiroMeOTAD exhibits a noticeable hypsochromic shift of the absorbance peaks for both donor and acceptor components (Figure 5A). This behavior is consistent with previous reports of Stark shifts of absorbance spectra of molecular dyes within surface-adsorbed monolayers that can be caused by an externally applied electric field or the ambient electric field associated with charge transfer across a dye monolayer.[43,44] However, for this system, the donor and acceptor absorbances

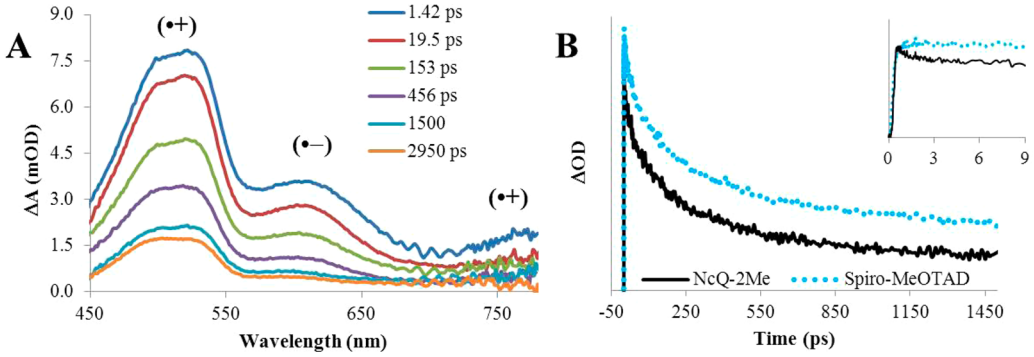

Figure 3. Laser flash photolysis of a thin film blend of NcQ-2Me and spiro-MeOTAD. A: Time resolved spectra. B: Monochromatic decay rates for the radical cation spiro-$MeOTAD^{(\bullet+)}$ at 500 nm, and for the radical anion NcQ-$2Me^{(\bullet-)}$ at 603 nm. Traces are normalized with respect to ΔOD at 740 fs. Inset: overlaid decay traces for initial 9 ps.

Table 2. Time Constants (τ) and Amplitudes (A) for Decay of the Radical Anion NcQ-2Me$^{(\bullet-)}$ (λ = 603 nm) and Radical Cation spiro-MeOTAD$^{(\bullet+)}$ (λ = at 500 nm) after Laser Flash Photolysis of a Thin Film Blend of NcQ-2Me/spiro-MeOTAD

species	τ_1/ps	$A_1 \times 10^4$	τ_2/ps	$A_2 \times 10^4$	τ_3/ps	$A_3 \times 10^4$	$A_{(\tau=\infty)} \times 10^4$
NcQ-2Me$^{(\bullet-)}$	0.77 ± 0.15	3.8	63 ± 6.3	7.0	550 ± 43	7.6	2.2
spiro-MeOTAD$^{(\bullet+)}$	n/a	n/a	97 ± 8.3	1.6	793 ± 89	1.5	8.6

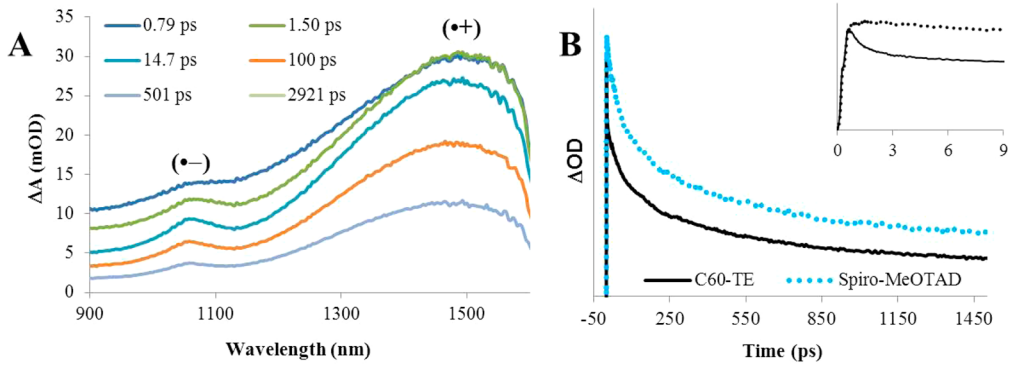

Figure 4. Laser flash photolysis of a thin film blend of C60-TE and spiro-MeOTAD. A: Time resolved spectra. B: Monochromatic decay rates for the radical cation spiro-MeOTAD$^{(\bullet+)}$ at 1500 nm, and for the radical anion C60-TE$^{(\bullet-)}$ at 1051 nm. Traces are normalized with respect to ΔOD at 563 fs. Inset: overlaid decay traces for initial 9 ps.

Table 3. Time Constants (τ) and Amplitudes (A) for Decay of the Radical Anion C60-TE$^{(\bullet-)}$ (λ = 1051 nm) and Radical Cation spiro-MeOTAD$^{(\bullet+)}$ (λ = 1500 nm) after Laser Flash Photolysis of a Thin Film Blend of C60-TE/spiro-MeOTAD

species	τ_1/ps	$A_1 \times 10^3$	τ_2/ps	$A_2 \times 10^3$	τ_3/ps	$A_3 \times 10^3$	τ_4/ps	$A_4 \times 10^3$	$A_{(\tau=\infty)} \times 10^4$
C60-TE$^{(\bullet-)}$	0.96 ± 0.1	2.7	30 ± 14	1.1	143 ± 70	1.6	802 ± 190	1.8	0.86
spiro-MeOTAD$^{(\bullet+)}$	n/a	n/a	n/a	n/a	55 ± 3.8	6.0	635 ± 42	6.1	3.0

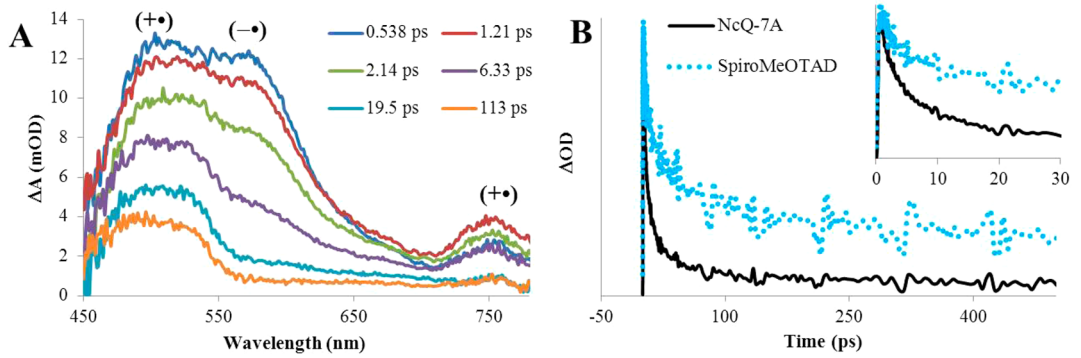

Figure 5. Laser flash photolysis of a ternary TiO_2/NcQ-7A/spiro-MeOTAD film consisting of rutile TiO_2 nanorods with surface chemisorbed NcQ-7A and spin-coated spiro-MeOTAD. A: Time resolved spectra. B: Monochromatic decay rates for the radical cation spiro-MeOTAD$^{(\bullet+)}$ at 490 nm, and for the radical anion NcQ-7A$^{(\bullet-)}$ at 600 nm, normalized with respect to ΔOD at 605 fs. Inset: overlaid decay traces for initial 30 ps.

Table 4. Time Constants (τ) and Amplitudes (A) for Decay of the Radical Anion NcQ-7A$^{(\bullet-)}$ (λ = 600 nm) and Radical Cation spiro-MeOTAD$^{(\bullet+)}$ (λ = 490 nm) after Laser Flash Photolysis of a Thin Film Blend of NcQ-7A/spiro-MeOTAD

species	τ_1/ps	$A_1 \times 10^3$	τ_2/ps	$A_2 \times 10^3$	τ_3/ps	$A_3 \times 10^3$	$A_{(\tau=\infty)} \times 10^4$
NcQ-7A$^{(\bullet-)}$	2.3 ± 0.18	2.8	17 ± 2.2	1.8	345 ± 88	0.3	0.14
spiro-MeOTAD$^{(\bullet+)}$	3.7 ± 0.97	2.0	46 ± 15	1.9	610 ± 210	1.0	0.80

remain far enough apart to disambiguate their decay kinetics. Each of the radical ion pair components decays multi-exponentially and at generally faster rates than for the corresponding NcQ-2Me/spiro-MeOTAD binary system. However, in the ternary system, we observe significantly faster decay for the radical anion component NcQ-7A$^{(\bullet-)}$ than for the radical cation spiro-MeOTAD$^{(\bullet+)}$ (Figure 5B, Table 4). The two fastest decay components of the radical anion decay are approximately twice as fast as the corresponding decay modes of the radical cation, and perhaps more important is the fact that the very fast decay component of the radical anion is more than half the total amplitude, whereas the corresponding decay component of the radical cation is only a third of the total decay amplitude. We infer from this result that there is a very fast decay mode for the radical anion that was not present in the binary system, and we assign that decay mode as the thermal electron transfer to TiO_2. An alternate explanation for the increased rapid decay of the radical anion could be the

dx.doi.org/10.1021/am502473q | ACS Appl. Mater. Interfaces 2014, 6, 10696−10705

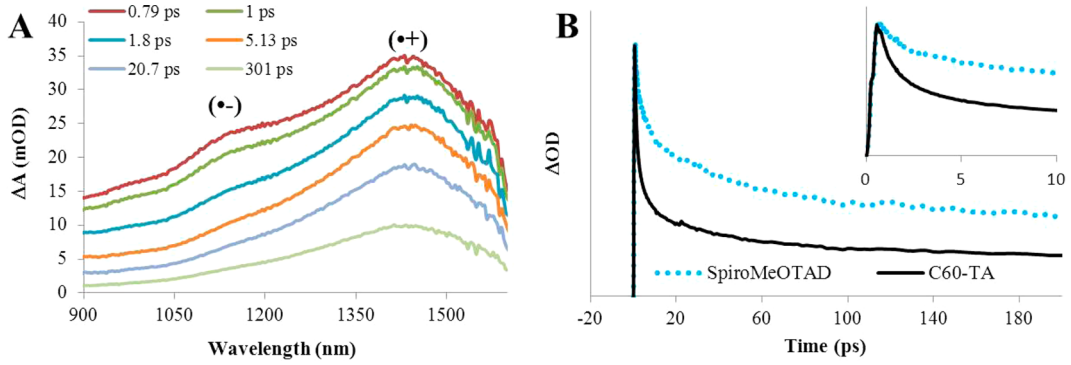

Figure 6. Laser flash photolysis of a ternary TiO_2/C60-TA/spiro-MeOTAD film consisting of rutile TiO_2 nanorods with surface chemisorbed C60-TA and spin-coated spiro-MeOTAD. A: Time resolved spectra. B: Monochromatic decay rates for the radical cation spiro-MeOTAD$^{(\bullet+)}$ at 1441 nm and for the radical anion C60-TA$^{(\bullet-)}$ at 1150 nm, normalized with respect to ΔOD at 560 fs. Inset: overlaid decay traces for initial 10 ps.

Table 5. Time Constants (τ) and Amplitudes (A) for Decay of the Radical Anion NcQ-7A$^{(\bullet-)}$ (λ = 600 nm) and Radical Cation spiro-MeOTAD$^{(\bullet+)}$ (λ = 490 nm) after Laser Flash Photolysis of a Thin Film Blend of NcQ-7A/spiro-MeOTAD

species	τ_1/ps	$A_1 \times 10^4$	τ_2/ps	$A_2 \times 10^4$	τ_3/ps	$A_3 \times 10^4$	$A_{(\tau=\infty)} \times 10^5$
C60TA$^{(\bullet-)}$	0.98 ± 0.06	9.2	15 ± 2.0	3.3	319 ± 45	1.5	1.3
spiro-MeOTAD$^{(\bullet+)}$	1.7 ± 0.18	6.1	33 ± 3.4	5.8	515 ± 55	3.4	3.3

presence of a higher local concentration of ambient O_2 within the ternary system, accounting for O_2 that is adsorbed onto the TiO_2 surface.[45] We discount this possibility because it should lead to a greatly increased proportion of radical cation that does not decay, and we do not observe any noticeable increase in the $\tau = \infty$ decay component for the spiro-MeOTAD$^{(\bullet+)}$ species between the corresponding binary and ternary systems. The accelerated decay rates for the radical cation in the ternary system indicate that recombination from the TiO_2 is faster than binary recombination between molecular donor−acceptor species, suggesting that in this solid state environment the TiO_2/spiro-MeOTAD recombination is not in the Marcus inverted kinetic region.

An estimation of the thermal injection rate can be obtained by subtracting the decay rates of the radical cation from those of the radical anion. This is a crude method because it neglects the contribution of long-range TiO_2/spiro-MeOTAD recombination to the early decay rate of the radical cation and does not consider the differences in the amplitudes of the decay rates. Equation 3 shows the decay half-life of the radical anion as the inverse sum of the bimolecular recombination and thermal injection rates (k_{CR-1} and k_{inj} from Figure 2):

$$\tau = \frac{1}{(k_{CR-1} + k_{inj})} \quad (3)$$

Solving for the injection rate gives

$$k_{inj} = \tau^{-1} - k_{CR-1} \quad (4)$$

If the decay rate of the spiro-MeOTAD is taken as k_{CR-1}, then the difference between the radical ion decay rates is the transfer rate for thermal electron injection from radical anion sensitizer to TiO_2. This analysis, applied separately to τ_1 and τ_2 of the NcQ-7A ternary system (Table 4) gives decay rates of 1.65×10^{11} s^{-1} (τ = 6 ps) and 3.7×10^{10} s^{-1} (τ = 27 ps) for the thermal electron injection process. For comparison, photoinduced electron transfer by neutral photoexcited sensitizers is reported to exhibit a multiexponential rate process with femtosecond and picosecond lifetime components, which are correlated to upper-excited or thermally equilibrated excited states, respectively.[12,13,46] Our data indicate that thermal electron injection by a radical anion sensitizer is kinetically similar to photoinduced electron injection by a thermally equilibrated photoexcited dye. However, given that the bimolecular recombination has similar decay rates to the thermal electron injection process, a clearer observation of the thermal electron injection might be obtained either by accelerating the injection rate or retarding the bimolecular recombination, perhaps through control over the orientation and/or distance between the molecular donor/acceptor pair.

An objective consideration of the kinetic behavior of the TiO_2/NcQ-7A/spiro-MeOTAD system must also consider the possibility that some photoinduced electron injection may have occurred. The neutral triplet excited state of NcQ-7A should be thermodynamically capable of electron injection into dry TiO_2 (Table 1); however, this process must compete with the acceptor-quenching of the dye by spiro-MeOTAD, which is complete within <1 ps. If the spiro-MeOTAD radical cation were formed as a result of multiple injection modes (photoinduced + photogalvanic), that could be an explanation for why some contingent of the radical cation decay is slower than the radical anion decay. However, if the spiro-MeOTAD radical cation were forming by thermal hole transfer from NcQ-7A$^{(\bullet+)}$ produced from photoinduced injection, we would not expect the rise time of spiro-MeOTAD$^{(\bullet+)}$ to match so closely as it does to the rise time of NcQ-7A$^{(\bullet-)}$.

For the ternary system including the trisadduct fullerene C60-TA, clear decay rates could not be determined because the ion pair absorbance peaks are too close together as a result of Stark shift caused by the ambient electric field of the charge-separated monolayer (Figure 6A). Overlay of the decay traces indicates that the early time decay of the radical anion (<5 ps) is a significantly greater component of its amplitude (65%) than for the radical cation (33%) (Table 5). This is likely an underestimation of the true contribution of the fast decay of C60-TA$^{(\bullet-)}$, because its longer time cannot be disambiguated from the decay of spiro-MeOTAD$^{(\bullet+)}$, so the true amplitudes of the longer decay times for C60-TA$^{(\bullet-)}$ are likely less than determined by fitting the data. Thermal electron injection

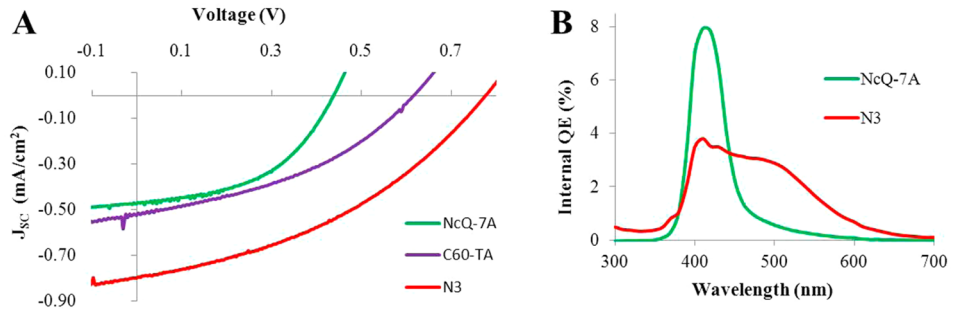

Figure 7. Current−voltage behavior of photoelectrochemical cells incorporating the acceptor-sensitizers NcQ-7A, C60-TA, and the ruthenium-based N3 dye. A: Solid-state photoelectrochemical cells using rutile TiO_2 nanorods as the oxide semiconductor photoanode and spiro-MeOTAD as a hole conductor layer. B: Liquid-junction photoelectrochemical cells using anatase TiO_2 nanoparticles as the oxide semiconductor photoanode and I^-/I_3^- as the redox shuttle.

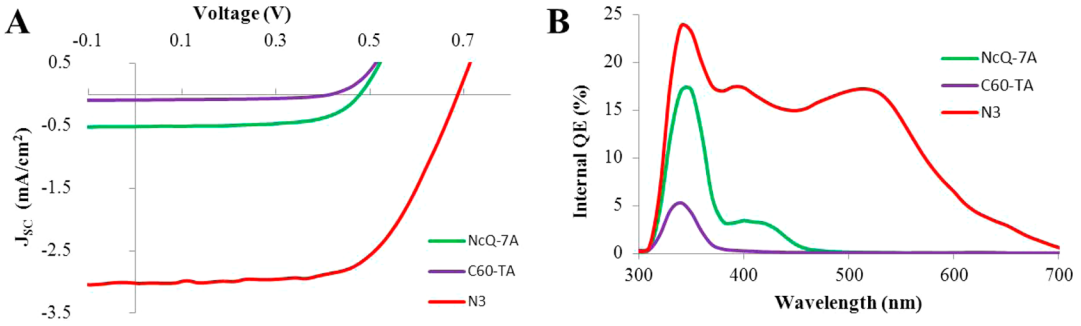

Figure 8. Current−voltage behavior (A) and internal quantum efficiency spectra (B) of liquid junction photoelectrochemical cells incorporating the acceptor-sensitizers NcQ-7A, C60-TA, and the ruthenium-based N3 dye.

within this system may be complete within 5−10 ps (Figure 6B, inset), but even a crude estimation is not possible here due to the extensive spectral overlap of the absorbances of the radical ion pair.

Photoelectrochemical Studies. Figure 7A shows the current−voltage behavior of solid-state photoelectrochemical cells incorporating the NcQ-7A and C60-TA sensitizers, along with the well-known ruthenium-based N3 dye. We utilized TiO_2 nanorods for the solid-state cells to avoid any difficulty in the infiltration of spiro-MeOTAD into the TiO_2. The solid-state P-DSC devices using NcQ-7A and C60-TA were competitive with a solid-state DSC using the N3 dye in terms of photocurrent density (Figure 7A), despite much weaker light absorption. Although the absorption range of NcQ-7A is much narrower than for N3 (Figure 7B and Supporting Information Figure S3), its higher quantum efficiency explains the competitive photocurrent of the device operating by the photogalvanic injection mechanism. Differences in the photovoltages among the solid-state devices are more difficult to explain. Attainment of the maximum possible open-circuit voltage (V_{OC}) depends on the quasi-Fermi level of the TiO_2: in the dark, it is pinned to the work function of the F-SnO_2 substrate, which is in turn pinned to the hole conductor (or redox electrolyte in liquid cells); under illumination, the TiO_2 quasi-Fermi level rises to just below the conduction band as the acceptor-states are populated with photocurrent.[32] If the photocurrent is very weak, the TiO_2 quasi-Fermi level may not rise to its maximum possible position. However, photocurrent difference between NcQ-7A and C60-TA is minimal, while photovoltage differs by more than 150 mV. The maximum possible V_{OC} of a solid-state dye-sensitized solar cell is modulated by the *tert*-butylpyridine that is included within the spiro-MeOTAD layer. The mechanism of this modulation is thought to be coordination of the *tert*-butylpyridine to exposed Ti atoms at the TiO_2 surface, and/or by deprotonation of the TiO_2 surface. If surface adsorption of the planar compact NcQ-7A dye allows less *tert*-butylpyridine to reach the oxide surface, then the effect of *tert*-butylpyridine would be diminished.

We previously identified charge-transfer dipoles as being a significant parameter in modifying photovoltage; however, we note that no such effect seems apparent here.[24] This discrepancy may be due to a screening effect of the charge transfer dipoles by $LiN(SO_2CF_3)_2$ present within the spiro-MeOTAD. Kinetics of such charge screening are in the microseconds time scale in liquid junction cells, where arrival of the screening ions from solution must be awaited.[43] In solid-state films, movement of ions through the spiro-MeOTAD matrix should be much slower, but during illumination, the zone near the TiO_2 surface will form a space-charge layer to which the $LiN(SO_2CF_3)_2$ would be drawn to accumulate. Modulation of this space-charge layer by salt ions is thought to retard recombination kinetics within solid-state DSCs relying on photoinduced charge injection,[47] but for P-DSCs, it may have the added effect of mitigating the photovoltage-enhancement of charge-transfer dipoles.

The current−voltage behavior of liquid-junction cells made with the dyes is shown in Figure 8. Liquid-junction cells were made using mesoporous anatase TiO_2 anodes prepared from a paste made from commercially available TiO_2 nanopowder, whereas the solid-state cells were made from hydrothermally grown rutile TiO_2 nanorods. The nanopowder-based paste used in this study provides mesoporous films that are not comparable to commercially available anatase TiO_2 pastes in terms of transparency and surface area but still give significantly

stronger light absorption than the rutile TiO_2 nanorod films. Despite the enhanced light absorption within the liquid-junction cells, the acceptor-sensitizers do not provide greater photocurrent compared to the solid-state cells, and the quantum efficiency spectra show that most of the obtained photocurrent for cells made with NcQ-7A and C60-TA actually derives from UV-absorption by the TiO_2. We attribute the poor photocurrent contribution from the acceptor-sensitizers to low yield of acceptor-quenching that provides the radical anion state of the sensitizers, and insufficient driving force for electron injection from their neutral photoexcited states. We note that the flat band potential of TiO_2 is elevated by ~500 mV in the presence of electrolyte compared to the dry state.[32] The average arrival time for the dissolved redox shuttle to a sensitizer monolayer has been estimated at ~1 μs,[48] and although naphthacenequinone and tris-adduct fullerenes do have microsecond lifetimes in degassed dilute solution (500 and 100 μs, respectively),[27,36] their excited state lifetimes are likely to be much shorter in the high concentration environment of the adsorbed dye monolayer due to additional excited state decay pathways such as triplet−triplet annihilation and triplet-charge annihilation.[49,50]

CONCLUSIONS

The results of this study support the assertion that acceptor-sensitizers operate via thermal electron injection from the radical anion state. The use of the solid-state dye solar cell system is advantageous to studies of thermal electron injection, because the close proximity of the primary electron donor ensures formation of the radical anion state of the sensitizer over other alternatives such as electron injection from the neutral excited state and/or nonradiative excited state decay. Solid-state dye-sensitized solar cells that operate in the photogalvanic mode have the potential to compete with cells exploiting direct photoinduced electron injection if acceptor-sensitizers can be identified with stronger absorption of visible light, especially for photoanodes with lower surface area such as the rutile TiO_2 nanorods employed in this study. Another opportunity that future acceptor-sensitizers may provide is a manner to probe the effective flat band potential in fully assembled solid-state photoelectrochemical cells via tandem spectroelectrochemistry of the oxide and sensitizer components.[51−54] Efforts in each of these directions are currently underway.

ASSOCIATED CONTENT

Supporting Information

Additional transient absorption data, SEM images of the TiO_2 nanorods, spectral characterization for NcQ-7A, and IPCE data for C60-TA. This material is available free of charge via the Internet at http://pubs.acs.org.

AUTHOR INFORMATION

Corresponding Author

*Email: youngblood@unt.edu.

Notes

The authors declare no competing financial interest.

ACKNOWLEDGMENTS

We acknowledge support from the University of North Texas (startup) and the National Science Foundation (CHE-0840518). We thank Prof. Francis D'Souza for assistance in conducting transient absorption data. We thank the UNT Center for Advanced Research and Technology (CART) for access to scanning electron microscopy instrumentation.

REFERENCES

(1) Rabinowitch, E. The Photogalvanic Effect I. The Photochemical Properties of the Thionine−Iron System. *J. Chem. Phys.* **1940**, *8*, 551−559.
(2) Rabinowitch, E. The Photogalvanic Effect II. The Photogalvanic Properties of the Thionine−Iron System. *J. Chem. Phys.* **1940**, *8*, 560−566.
(3) Alberry, W. J. Development of Photogalvanic Cells for Solar Energy. *Acc. Chem. Res.* **1982**, *15*, 142−148.
(4) Kippelen, B.; Brédas, J.-L. Organic Photovoltaics. *Energy Environ. Sci.* **2009**, *2*, 251−261.
(5) Hagfeldt, A.; Boschloo, G.; Sun, L.; Kloo, L.; Pettersson, H. Dye-Sensitized Solar Cells. *Chem. Rev.* **2010**, *110*.
(6) O'Regan, B.; Gratzel, M. A Low-Cost, High-Efficiency Solar Cell Based on Dye-Sensitized Colloidal TiO_2 films. *Nature* **1991**, *353*, 737−740.
(7) Ortmans, I.; Moucheron, C.; Kirsch-De Mesmaeker, A. Ru(II)polypyridine Complexes with a High Oxidation Power. Comparison between Their Photoelectrochemistry with Transparent SnO_2 and Their Photochemistry with Desoxyribonucleic Acids. *Coord. Chem. Rev.* **1998**, *168*, 233−271.
(8) Thompson, D. W.; Kelly, C. A.; Farzad, F.; Meyer, G. J. Sensitization of Nanocrystalline TiO_2 Initiated by Reductive Quenching of Molecular Excited States. *Langmuir* **1999**, *15*, 650−653.
(9) Kleverlaan, C.; Alebbi, M.; Argazzi, R.; Bignozzi, C. A.; Hasselmann, G. M.; Meyer, A. Molecular Rectification by a Bimetallic Ru-Os Compound Anchored to Nanocrystallin TiO_2. *Inorg. Chem.* **2000**, *39*, 1342−1343.
(10) Kleverlaan, C.; Indelli, M. T.; Bignozzi, C. A.; Pavanin, L.; Scandola, F.; Hasselmann, G. M.; Meyer, G. J. Stepwise Charge Separation in Heterotriads. Binuclear Ru(II)-Rh(III) Complexes on Nanocrystalline Titanium Dioxide. *J. Am. Chem. Soc.* **2000**, *122*, 2840−2849.
(11) Hu, K.; Robson, K. C. D.; Johansson, P. G.; Berlinguette, C. P.; Meyer, G. J. Intramolecular Hole Transfer at Sensitized TiO_2 Interfaces. *J. Am. Chem. Soc.* **2012**, *134*, 8352−8355.
(12) Kuciauskas, D.; Monat, J. E.; Villahermosa, R.; Gray, H. B.; Lewis, N. S.; McCusker, J. K. Transient Absorption Spectroscopy of Ruthenium and Osmium Polypyridyl Complexes Adsorbed onto Nanocrystalline TiO2 Photoelectrodes. *J. Phys. Chem. B* **2002**, *106*, 9347−9358.
(13) Benkö, G.; Kallioinen, J.; Korppi-Tommola, J. E. I.; Yartsev, A. P.; Sundström, V. Photoinduced Ultrafast Dye-to-Semiconductor Electron Injection from Nonthermalized and Thermalized Donor States. *J. Am. Chem. Soc.* **2002**, *124*, 489−493.
(14) Dos Santos, T.; Morandeira, A.; Koops, S.; Mozer, A. J.; Tsekouras, G.; Dong, Y.; Wagner, P.; Wallace, G.; Earles, J. C.; Gordon, K. C.; Officer, D.; Durrant, J. R. Injection Limitations in a Series of Porphyrin Dye-Sensitized Solar Cells. *J. Phys. Chem. C* **2010**, *114*, 3276−3279.
(15) Jensen, R. A.; Ryswyk, H. V.; She, C.; Szarko, J. M.; Chen, L. X.; Hupp, J. T. Dye Sensitized Solar Cells: Sensitizer-Dependent Injection into ZnO Nanotube Electrodes. *Langmuir* **2010**, *26*, 1401−1404.
(16) Eu, S.; Katoh, T.; Umeyama, T.; Matano, Y.; Imahori, H. Synthesis of Sterically Hindered Phthalocyanines and Their Applications to Dye-Sensitized Solar Cells. *Dalton Trans.* **2008**, 5476−5483.
(17) Morandeira, A.; López-Duarte, I.; Martínez-Díaz, M. V.; O'Regan, B.; Shuttle, C.; Haji-Zainulabidin, N. A.; Torres, T.; Palomares, E.; Durrant, J. R. Slow Electron Injection on Ru-Phthalocyanine Sensitized TiO_2. *J. Am. Chem. Soc.* **2007**, *129*, 9250−9251.

(18) Clark, C. C.; Marton, A.; Meyer, G. J. Evidence for Static Quenching of MLCT Excited States by Iodide. *Inorg. Chem.* **2005**, *44*, 3383−3385.
(19) Clark, C. C.; Marton, A.; Srinivasan, R.; Sarjeant, A. A. N.; Meyer, G. J. Triiodide Quenching of Ruthenium MLCT Excited State in Solution and on TiO_2 Surfaces: An Alternate Pathway for Charge Recombination. *Inorg. Chem.* **2006**, *45*, 4728−4734.
(20) Marton, A.; Clark, C. C.; Srinivasan, R.; Freundlich, R. E.; Sarjeant, A. A. N.; Meyer, G. J. Static and Dynamic Quenching of Ru(II) Polypyridyl Excited States by Iodide. *Inorg. Chem.* **2006**, *45*, 362−369.
(21) Cappel, U. B.; Karlsson, M. H.; Pschirer, N. G.; Eickemeyer, F.; Schoneboom, J.; Erk, P.; Boschloo, G.; Hagfeldt, A. A Broadly Absorbing Perylene Dye for Solid-State Dye-Sensitized Solar Cells. *J. Phys. Chem. C* **2009**, *113*, 14595−14597.
(22) Cappel, U. B.; Smeigh, A. L.; Plogmaker, S.; Johansson, E. M. J.; Rensmo, H.; Hammarström, L.; Hagfeldt, A.; Boschloo, G. Characterization of the Interface Properties and Processes in Solid State Dye-Sensitized Solar Cells Employing a Perylene Sensitizer. *J. Phys. Chem. B* **2011**, *115*, 4345−4358.
(23) Kc, C. B.; Stranius, K.; D'Souza, P.; Subbaiyan, N. K.; Lemmetyinen, H.; Tkachenko, N. V.; D'Souza, F. Sequential Photoinduced Energy and Electron Transfer Directed Improved Performance of the Supramolecular Solar Cell of a Zinc Porphyrin−Zinc Phthalocyanine Conjugate Modified TiO_2 Surface. *J. Phys. Chem. C* **2013**, *117*, 763−773.
(24) Berhe, S. A.; Zhou, J. Y.; Haynes, K. M.; Rodriguez, M. T.; Youngblood, W. J. Electron Transport in Acceptor-Sensitized Polymer−Oxide Solar Cells: The Importance of Surface Dipoles and Electron Cascade Effects. *ACS Appl. Mater. Interfaces* **2012**, *4*, 2955−2963.
(25) Haris, S. P.; Zhang, Y.; Le Bourdonnec, B.; McCurdy, C. R.; Portoghese, P. S. O-Naphthalenedicarboxaldehyde Derivative of 7′-Aminonaltrindole as a Selective Δ-Opioid Receptor Affinity Label. *J. Med. Chem.* **2007**, *50*, 3392−3396.
(26) Berhe, S. A.; Nag, S.; Molinets, Z.; Youngblood, W. J. Influence of Seeding and Bath Conditions in Hydrothermal Growth of Very Thin (∼20 nm) Single-Crystalline Rutile TiO_2 Nanorod Films. *ACS Appl. Mater. Interfaces* **2013**, *5*, 1181−1185.
(27) Guldi, D. M.; Asmus, K.-D. Photophysical Properties of Mono- and Multiply-Functionalized Fullerene Derivatives. *J. Phys. Chem. A* **1997**, *101*, 1472−1481.
(28) Yamaji, M.; Takehira, K.; Itoh, T.; Shizuka, H.; Tobita, S. Photophysical and Photochemical Properties of 1,4-Tetracenequinone in Solution. *Phys. Chem. Chem. Phys.* **2001**, *3*, 5470−5474.
(29) Roberts, L. W.; Schuster, G. B. Synthesis and Study of Naphthacenedione (TQ) as a Photosensitizer for One-Electron Oxidation of DNA. *Org. Lett.* **2004**, *6*, 3813−3816.
(30) Guldi, D. M.; Hungerbuhler, H.; Asmus, K.-D. Redox and Excitation Studies with C60-Substituted Malonic Acid Diethyl Esters. *J. Phys. Chem.* **1995**, *99*, 9380−9385.
(31) Liu, Y.; Scully, S. R.; McGehee, M. D.; Liu, J.; Luscombe, C. K.; Frechet, J. M. J.; Shaheen, S. E.; Ginley, D. S. Dependence of Band Offset and Open-Circuit Voltage on the Interfacial Interaction between TiO_2 and Carboxylated Polythiophenes. *J. Phys. Chem. B* **2006**, *110*, 3257−3261.
(32) Cahen, D.; Hodes, G.; Gratzel, M.; Guillemoles, J. F.; Riess, I. Nature of Photovoltaic Action in Dye-Sensitized Solar Cells. *J. Phys. Chem. B* **2000**, *104*, 2053−2059.
(33) Pavlishchuk, V. V.; Addison, A. W. Converstion Constants for Redox Potentials Measured versus Different Reference Electrodes in Acetonitrile Solutions at 25 °C. *Inorg. Chim. Acta* **2000**, *298*, 97−102.
(34) Bredas, J. L.; Silbey, R.; Boudreaux, D. S.; Chance, R. R. Chain-Length Dependence of Electronic and Electrochemical Properties of Conjugated Systems: Polyacetylene, Polyphenylene, Polythiophene, and Polypyrrole. *J. Am. Chem. Soc.* **1983**, *105*, 6555−6559.
(35) Braslavsky, S. E. Glossary of Terms Used in Photochemistry, (IUPAC Recommendations 2006). *Pure Appl. Chem.* **2007**, *79*, 293−465.
(36) Yamaji, M.; Itoh, T.; Tobita, S. Photochemical Properties of the Triplet π,π^* State, Anion and Ketyl Radicals of 5,12-Naphthacenequinone in Solution Studied by Laser Flash Photolysis: Electron Transfer and Phenolic H-Atom Transfer. *Photochem. Photobiol. Sci.* **2002**, *1*, 869−876.
(37) Olson, C.; Veldman, D.; Bakker, K.; Lenzmann, F. Characterization of the Pore Filling of Solid State Dye Sensitized Solar Cells with Photoinduced Absorption Spectroscopy. *Int. J. Photoenergy* **2011**, *2011*, 513089.
(38) Cappel, U. B.; Gibson, E. A.; Hagfeldt, A.; Boschloo, G. Dye Regeneration by Spiro-MeOTAD in Solid State Dye-Sensitized Solar Cells Studied by Photoinduced Absorption Spectroscopy and Spectroelectrochemistry. *J. Phys. Chem. C* **2009**, *113*, 6275−6281.
(39) Fukuzumi, S.; Ohkubo, K.; Imahori, H.; Guldi, D. M. Driving Force Dependence of Intermolecular Electron-Transfer Reactions of Fullerenes. *Chem.—Eur. J.* **2003**, *9*, 1585−1593.
(40) Wasielewski, M. R.; Johnson, D. G.; Svec, W. A. Photoinduced Electron Transfer in Fixed Distance Chlorophyll−Quinone Donor−Acceptor Molecules. In *Supramolecular Photochemistry*; Springer, 1987; pp 255−266.
(41) Marcus, R. A.; Sutin, N. Electron Transfers in Chemistry and Biology. *Biochim. Biophys. Acta* **1985**, *811*, 265−322.
(42) Verhoeven, J. W. On the Role of Spin Correlation in the Formation, Decay, and Detection of Long-Lived, Intramolecular Charge-Transfer States. *J. Photochem. Photobiol. C: Photochem. Rev.* **2006**, *7*, 40−60.
(43) Ardo, S.; Sun, Y.; Staniszewski, A.; Castellano, F. N.; Meyer, G. J. Stark Effects after Excited-State Interfacial Electron Transfer at Sensitized TiO_2 Nanocrystallites. *J. Am. Chem. Soc.* **2010**, *132*, 6696−6709.
(44) Cappel, U. B.; Feldt, S. M.; Schöneboom, J.; Hagfeldt, A.; Boschloo, G. The Influence of Local Electric Fields on Photoinduced Absorption in Dye-Sensitized Solar Cells. *J. Am. Chem. Soc.* **2010**, *132*, 9096−9101.
(45) Linsebigler, A. L.; Lu, G.; Yates, J. T. Photocatalysis on TiO_2 Surfaces: Principles, Mechanisms, and Selected Results. *Chem. Rev.* **1995**, *95*, 735−758.
(46) Haque, S. A.; Palomares, E.; Cho, B. M.; Green, A. N. M.; Hirata, N.; Klug, D. R.; Durrant, J. R. Charge Separation versus Recombination in Dye-Sensitized Nanocrystalline Solar Cells: The Minimization of Kinetic Redundancy. *J. Am. Chem. Soc.* **2005**, *127*, 3456−3462.
(47) Kruger, J.; Plass, R.; Cevey, L.; Piccirelli, M.; Gratzel, M.; Bach, U. High Efficiency Solid-State Photovoltaic Device due to Inhibition of Interface Charge Recombination. *Appl. Phys. Lett.* **2001**, *79*, 2085−2087.
(48) Listorti, A.; O'Regan, B.; Durrant, J. R. Electron Transfer Dynamics in Dye-Sensitized Solar Cells. *Chem. Mater.* **2011**, *23*, 3381−3399.
(49) Shao, M.; Yan, L.; Li, M.; Hu, B. Triplet−Charge Annihilation versus Triplet−Triplet Annihilation in Organic Semiconductors. *J. Mater. Chem. C* **2013**, *1*, 1330−1336.
(50) Thompson, N. J.; Hontz, E.; Congreve, D. N.; Bahlke, M. E.; Reineke, S.; Van Voorhis, T.; Baldo, M. A. Nanostructured Singlet Fission Photovoltaics Subject to Triplet-Charge Annihilation. *Adv. Mater.* **2013**, *26*, 1366−1371.
(51) Bonifas, A. P.; McCreery, R. L. Solid State Spectroelectrochemistry of Redox Reactions in Polypyrrole/Oxide Molecular Heterojunctions. *Anal. Chem.* **2012**, *84*, 2459−2465.
(52) Rothenberger, G.; Fitzmaurice, D.; Gratzel, M. Spectroscopy of Conduction Band Electrons in Transparent Metal Oxide Semiconductor Films: Optical Determination of the Flatband Potential of Colloidal Titanium Dioxide Films. *J. Phys. Chem.* **1992**, *96*, 5983−5986.
(53) Redmond, G.; Fitzmaurice, D. Spectroscopic Determination of Flatband Potentials for Polycrystalline TiO_2 Electrodes in Nonaqueous Solvents. *J. Phys. Chem.* **1993**, *97*, 1426−1430.

(54) Boschloo, G.; Fitzmaurice, D. Spectroelectrochemical Investigation of Surface States in Nanostructured TiO_2 Electrodes. *J. Phys. Chem. B* **1999**, *103*, 2228−2231.